Journal of Korean Association of Crystal Growth
Vol. 7, No. 1 (1997) 81-92

1-Dimensional efficiency modeling of rear floationg junction solar cell

A.U. Ebong, D.S. Kim and S.H. Lee
Photovoltaics Team, Electronic Materials Laboratory, Materials Sector, Samsung Advanced Institute of Technology, P.O.Box 111, Suwon 440-600, Korea

후면부유접합 태양전지에 있어서의 1차원 효율 모델링

A.U. Ebong, 김동섭, 이수홍
삼성종합기술원 재료섹터, 전자재료Lab., 태양전지팀, 수원우체국 사서함 111, 수원, 400-600

Abstract Rear floating junction cell (RFJC), using the buried contact technology, is capable of eliminating the efficiency limitations on the single sided cells by providing betterear surface passivation. The implementation of this structure, is simpler and lower in cost and therefore viable for commercial production. However, the contributions, due to damages in the two sets of grooves, to the total dark saturation current density has limited the achievable efficiency of the RFJC to only 21.5 %. This paper reports on the efficiency estimates of RFJC using PC-1D.

요 약 전극함몰형 태양전지에 후면 부유접합의 도입은 양질의 표면보호를 제공할 수 있어서 효율 향상을 꾀할 수 있다. 이 논문은 PC-1D 모델링을 통하여 후면 부유접합형 태양전지의 효율을 시뮬레이션 분석한 것이다.

1. Introduction

The electrical output characteristics, especially the open circuit voltage, of a solar cell can be improved by reducing the dark saturation current contribution from the back side of the cell. The rear surface of the single sided buried contact (SSBC) cells is normally covered with metal and therefore contributes greatly to the dark saturation current and a high back surface recombination velocity. This, in effect, reduces the open cir-

cuit voltage of the cells and hence the efficiency.

It is well known that the performance of a solar cell can be improved if the rear surface is well passivated with a very high quality oxide, as in the case of the PERL (passivated emitter, rear locally diffused) structure [1]. Even though the oxide passivation has shown, some improvement over the BSF (back surface field) normally used, the oxide passivation has been found to be more effective on n-type surfaces than p-type substrates. This behavior is due to the high σ_n/σ_p ratio [2], where σ_n and σ_p are the electron and hole capture cross sections respectively. The positive oxide charges attract majority carriers ("accumulation") and repel minority carriers for an n-type layer at the surface. Therefore, the effective surface recombination velocity decreases with increasing values of the positive fixed oxide charge density, Q_f, due to the increasing n_s/p_s ratio, where n_s and p_s are the carrier densities of electrons and holes at the semiconductor surfaces.

The dark saturation current on the rear of a cell can be further reduced when high quality oxide is grown on an n-type diffused surface and this surface is not contacted. This is the case of the RFJC (adopted in this work because it is easier to diffuse phosphorus simultaneously into the rear surface and front surface rather than diffusing boron across the entire rear surface) in which the n-type diffused surface on the rear is not contacted. The features of the RFJC structure, Fig. 1, are a passivating silicon dioxide

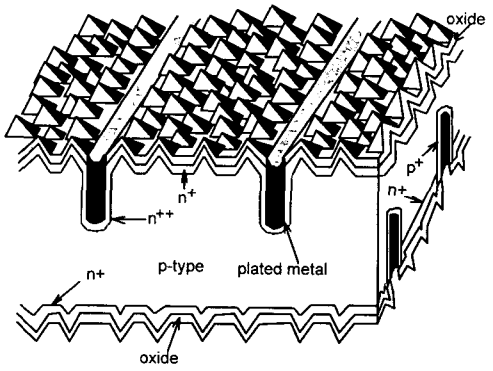

Fig. 1. Features of RFDS solar cell.

layer on both surfaces, a lightly diffused phosphorus emitter on the front and rear, groove fingers on both front and rear, with heavy, deep diffusions underneath the front and rear metal grids for low contact recombination. The RFJC is bifacial in nature which offers improved energy collection in the field due to its ability to respond to light incident on the rear surface [3]. Also, because of the improved rear surface passivation, the cells can be fabricated on a wide range of substrate resistivity [4].

The structure in the dark, is identical to the npn bipolar transistor with a floating collector. The base of the transistor corresponds to the substrate (P), the emitter to the n^+ front region and the collector to the n^+ (non contacted) region on the rear.

2. Advantages of RFJC over the SSBC structure

The advantages of RFJC over SSBC cells include, simplicity and lower cost, higher open circuit capability, higher conversion ef-

ficiency capability and substrate resistivity independence.

2.1. Simpler and Lower cost

The double sided buried contact processing sequence is simpler and shorter since the lengthy sintering step for the SSBC structure is eliminated. The elimination of the vacuum evaporator, which is often used to deposit aluminum on the rear surface is expected to significantly reduce the production costs. Since grooves are on both sides of the RFJC, the cost of plating a finger is lower than that of SSBC cells which have the whole rear covered with metal.

2.2. Higher open circuit voltage capability

The deliberate diffusion of phosphorus to the front and rear surfaces followed by the growth of a good quality oxide results in a double passivation of both the front and rear surfaces. This, in effect, reduces surface recombination to values well below the Al-sintered rear of the BSF cells. The rear surface therefore has very little contribution to the dark saturation current of the cell which, as noted earlier, is the major draw back to the single sided structure.

The improved rear surface passivation has enabled the RFJC structure to demonstrate an open circuit voltage in excess of 670 mV [5,6] on 1 Ω. cm, p-type substrate for front illumination and almost 670 mV for the independent rear illumination. This represents a 26 mV increase on the open circuit voltage obtained for the SSBC structure on a similar substrate resistivity.

2.3. Higher conversion efficiency capability

The RFJC is capable of achieving a 10 % relative advantage in conversion efficiency over the standard sequence [5] primarily because of the relatively low rear surface recombination velocity. It also offers improved energy collection in the field due to its ability to respond to light incident on the rear surface. Short circuit current densities measured in experimental RFJC illuminated from the rear have been only marginally lower than those measured when illuminated from the front [6]. Two opportunities arise from this feature. One is that modules can be designed with transparent rear surfaces allowing them to collect primarily diffuse light on the module rear [7]. Another advantage of the RFJC is that the effective concentration ratio obtained from stationary (nontracking) concentrators can be significantly increased for a cell responsive to light from both surfaces.

2.4. Substrate resistivity independence

The double sided buried contact cell does not depend on substrate resistivity for its performance i.e. it is suitable for a wider range of substrate resistivities than SSBC structure whose poor rear surface gives a bias towards lower substrate resistivities for improved performance. This effect has been demonstrated elsewhere [4] in which vari-

ous substrate resistivities were used and in each case the RFJC open circuit voltage (V_{oc}) was higher than that obtained with the SSBC structure.

3. 1-Dimensional analysis of the RFJC

The analysis of the rear floating emitter is based on Ebers-Moll model of the n^+pn^+ bipolar junction transistor. Figure 2 shows the Ebers-Moll equivalent circuit for the structure in consideration. The associated equations are given according to Sze [8]. The Ebers-Moll model is used for the RFJC because it gives a quick understanding of the structure. This is particularly useful in explaining the effect of the interface shunt conductance across the rear floating junction on the fill factor of RFJC as given by Ebong et al [9] and Ghanam [17].

The diode currents I_F and I_R are as follows

$$I_F = I_{FO}(e^{qV_{BE}/KT}-1) \quad (1)$$

$$I_R = I_{RO}(e^{qV_{BC}/KT}-1) \quad (2)$$

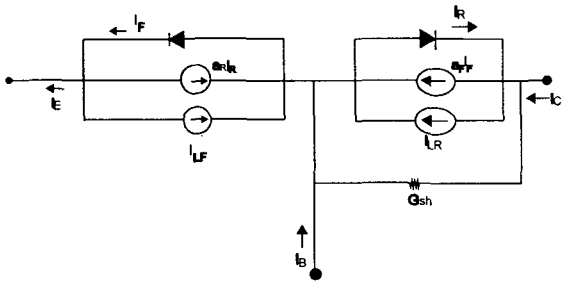

Fig. 2. Ebers-Moll equivalent circuit for RFDS cells (note $a_F=\alpha_F$, and $a_R=\alpha_R$ and $G_{sh}=0$).

where I_{FO} and I_{RO} are the saturation currents of the normally forward and reverse biased diodes, respectively. The terminal currents are

$$I_E = I_F-\alpha_F I_R \quad (3)$$

$$I_C = \alpha_F I_F-I_R \quad (4)$$

$$I_B = I_E-I_C=(1-\alpha_F)I_F+(1-\alpha_R)I_R \quad (5)$$

Where α_F is the forward common-base current gain and α_R is the reverse common-base current gain.

By combining equations 1 through 4, the general equations for the basic Ebers-moll model can be derived

$$I_E = I_{FO}(e^{qV_{BE}/KT}-1)-\alpha_R I_{RO}(e^{qV_{BC}/KT}-1) \quad (6)$$

$$I_C = \alpha_F I_{FO}(e^{qV_{BE}/KT}-1)-I_{RO}(e^{qV_{BC}/KT}-1) \quad (7)$$

$$I_B = (1-\alpha_F)I_{FO}(e^{qV_{BE}/KT}-1)+(1-\alpha_R)I_{RO}(e^{qV_{BC}/KT}-1) \quad (8)$$

Equations 6 through 8 are the terminal currents in which I_E, I_C and I_B represent the emitter, collector and base current respectively.

The coefficients I_{FO} and I_{RO} can be obtained from the measurements of I_{EO} and I_{CO}, where I_{EO} is the measured reverse-saturation current of the emitter-base junction with the collector short-circuited (i.e. $V_{BC}=0$ and V_{BE} is large and negative) and I_{CO} is the measured reverse-saturation current of the colector-base junction with the emitter

short-circuited (i.e. $V_{BE}=0$ and V_{BC} is large and negative).

Using these two conditions the coefficients are found

$$I_{FO} = -I_{EO} \tag{9}$$

$$I_{RO} = I_{CO} \tag{10}$$

Substituting 9 and 10 in 6 and 7 to derive the emitter and the collector current equations

$$I_E = -I_{EO}(e^{qV_{BE}/KT}-1) - \alpha_R I_{CO}(e^{qV_{BC}/KT}-1) \tag{11}$$

$$I_C = -\alpha_F I_{EO}(e^{qV_{BC}/KT}-1) - I_{CO}(e^{qV_{BE}/KT}-1) \tag{12}$$

An important reciprocity relationship is that

$$\alpha_F I_{EO} = \alpha_R I_{CO} \tag{13}$$

Since the collector region of the transistor is not contacted (floating), the collector current I_C is always zero. In such case equation 12 leads to

$$(e^{qV_{BC}/KT}-1) = \frac{\alpha_F I_{EO}}{I_{CO}}(e^{qV_{BE}/KT}-1) = \alpha_R (e^{qV_{BE}/KT}-1) \tag{14}$$

This result indicates that when the emitter base junction is forward-biased a forward bias potential is built up at the floating collector-base junction. The variation of emitter and collector base voltages is modeled numerically using PC-1D [10] and is given in Fig. 3.

4. Recombination estimates for RFJC

The theoretical limits of the RFJC is based on PERL cell. The RFJC cell is similar to PERL in the following respects. Firstly, both structures have thermally oxidized front and rear surfaces. Secondly, the rear floating junction (non contacted n-layer on rear) in the case of RFJC is akin to the aluminum rear for the PERL cells in reducing the rear surface contribution to the dark saturation current. While RFJC have diffused n-type layer, the PERL cells have electrostatically induced n-layer which appears along the rear surface of the device under illumination. The main difference between the two structures is the grooves and the dots on the rear for the RFJC and PERL cells respectively. Therefore the J_o (dark saturation current density) contribution by the grooves

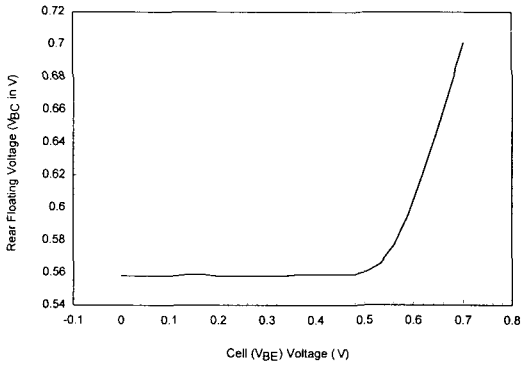

Fig. 3. Variation of emitter with collector base voltage as modeled numerically using PC-1D.

must be included in the efficiency estimate of the RFJC cell.

The saturation current density (J_o) in the RFJC is made up of contributions from the diffused emitter and top surface ($J_{o\text{-emitter}}$), The back surface ($J_{o\text{-rear}}$), the grooves on the front of the cell ($J_{o\text{-front-grooves}}$), the bulk ($J_{o\text{-bulk}}$), the edges and the diffused rear grooves ($J_{o\text{-rear-grooves}}$). Values for the saturation current from the emitter and bulk can be estimated by comparison with PERL cell while the top surface groove contributions can be extracted from earlier work with high voltage buried contact cell [11]. The rear surface groove contributions are estimated by the use of PC-1D in conjunction with the Sproul's work [12]. An ideality factor of 1 is assumed for the rest of the calculations. A summary of the various comp-onents of the dark saturation current density is given in Table 1.

Table 1
Theoretical estimate of saturation current density (J_o) for the RFJC cells

Component	Minimum value (A/cm^2)	Maximum value (A/cm^2)
Emitter including top surface	2.7×10^{-14}	4×10^{-14}
Top grooves	2.5×10^{-14}	3.1×10^{-14}
Bulk		2×10^{-14}
Back surface	2×10^{-14}	4×10^{-14}
Rear grooves	9×10^{-14}	1.3×10^{-13}

5. Efficiency estimate using PC-1D and groove recombination

The assumptions used in efficiency modeling of RFJC are diffusion length of 1.35 mm (this value corresponds to experimentally measured value from the best PERL cell fabricated on 1 ohm cm, float zone, p-type substrate); same values for front and rear surface recombination velocities are used since both surfaces have the same phosphorus diffusion and oxidation; large shunt and zero series resistance and other device parameters used in the modeling are outlined in Table 2 and are chosen to correspond to a realistic device. Note that the 1-dimensional modeling cannot include the rear grooves as such a separate calculation is used. That is, the modeling is done in two steps, one for the light diffusion and the other for the groove diffusion.

The modeling results are summarized in Table 3. Based on the practically measured fill factor of 81.2 % [13] and the results of Table 3, The maximum realistic efficiency for this structure is 23 %.

The results of Table 3 are of the assumption that there are no losses in the device. For a practical estimate based on the experimental results for the RFJC, recombination in various parts of the device has to be taken into account, particularly in regions such as the grooves which are not common to more standard cell designs.

From Table 3, using an effective surface recombination velocity of 100 cm/s (which is a practically measured value [6], $J_{o\text{-total}}$

Table 2
PC-1D Modeling Parameters for RFJC

Parameter	Value
Base substrate	p-type
Substrate thickness (μm)	280
Top diffusion	n-type
Surface concentration(cm^{-3})	3×10^{18}
Profile	Gaussian
Diffusion depth (μm)	1.088
ρ(Ω/square)	239.4
Rear diffusion	n-type
Surface concentration(cm^{-3})	3×10^{18}
Profile	Gaussian
Diffusion depth (μm)	0.5788
ρ(Ω/square)	450
Spectrum	AM 1.5G
Intensity (W/cm^2)	0.1
Average incident angle	41.5°
Band gap narrowing	18.7 meV at 7×10^{17} cm^{-3} (donor) 18.1 meV at 1×10^{17} cm^{-3} (acceptor)
Temperature	300 K
Internal surface reflectance	92 % (front), 97 % (rear)
Metal shading/ reflection	3 %
Light trapping	Textured (facet angle 55°)

can be calculated as 6.28×10^{-14} A/cm^2. As shown in Table 1, the groove contribution is 2.8×10^{-14} A/cm^2. Since there are two sets of grooves (front and rear), the total contribution from the grooves is likely to be twice this value i. e. $J_{o-grooves}=5.6\times10^{-14}$ A/cm^2 assuming similar contributions from n and ptype grooves. With this addition, a new estimate of $J_{o-total}$ is made as 1.198×10^{-13} A/cm^2. This results in an efficiency of 22.9 %, V_{oc} of 686.6 mV and 83.4 % fill factor. To estimate a more practical efficiency value for the RFJC, all the possible losses must be taken into account. Thus, the shading losses from the front metal contact is estimated and used in the efficiency estimate.

Table 3
The results of the PC-1D modeling for 1 $\Omega\cdot$cm substrate as a function of front and rear surface recombination velocity

V_{OC} (mV)	J_{SC} (mA/cm^2)	η (%)	FF (%)	S_n,S_h (cm/s)
705.7	40.2	23.6	83.2	10
704.4	40.2	23.6	83.3	50
703	40.2	23.6	83.5	100
700	40.2	23.5	83.5	200
697	40.1	23.4	83.7	400
695.2	40.1	23.3	83.6	600
691.3	40.1	23.2	83.6	800
689.5	40.1	23.1	83.6	1000

6. Front contact design

To approach the predicted levels for the RFJC, parasitic resistance and shading losses need to be minimized. The front contact (Fig. 4) design takes account of the trade off between shading losses, resistive losses in the diffused layer and deterioration of the

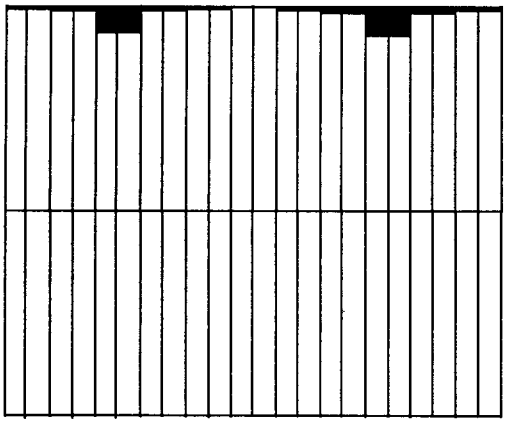

Fig. 4. Front finger (groove) design for the RFJC.

short wavelength response that accompanies heavier diffusions. Other losses like the series resistance of the metal lines and the contact resistance between these lines and silicon are not considered since they are small with the buried contact technology because of the control of the groove diffusion, groove geometry and the aspect ratio independent of other losses [14]. The initial front contact design for RFJC assumed a sheet resistivity (ρ_s) of 100 ohm/square with the fractional power loss in the diffused layer (P_{dl}) given by [15]

$$P_{dl} = S^2 J_{MP} \rho_S / 12 V_{MP} \quad (15)$$

where ρ_s is the sheet resistivity of the top surface, S is the finger spacing, J_{MP} and V_{MP} are the current density and voltage respectively at the maximum power point.

For 30 μm wide fingers (which is a typical width obtained from mechanically scribed grooves) with an additional allowance for 1 % shading loss in the bus bar and contact pads, the total shading loss fraction (P_{sl}) is given by

$$P_{sl} = 0.01 + 0.003/S \quad (16)$$

for finger spacing S in centimeters.

The power loss due to the ohmic resistance of the metal fingers is given by [15]

$$P_f = \frac{J_{MP}\rho_m}{3A_f V_{MP}} L^2 (s - w_f) \quad (17)$$

where L is the length of the finger, ρ_m is the resistivity of metal, A_f is the cross sectional area of finger, s is the center-to-center distance between adjacent fingers and W_f is the width of the finger.

By combining equations 15, 16 and 17, the power loss to be minimized is given by

$$P = P_{dl} + P_{sl} + P_f \quad (18)$$

Substituting the values of P_{dl}, P_{sl} and P_f and taking the first derivative of P with respect to S gives

$$\frac{dP}{dS} = \frac{\rho_s J_{MP} S}{6 V_{MP}} - \frac{0.003}{S^2} + \frac{J_{MP}\rho_m}{3A_f V_{MP}} L^2 \quad (19)$$

which is zero when

$S = 1.25$ mm

Substituting back into equations 15 and 16 give

$P_{dl} = 0.080$ or 0.8 %

$P_{sl}=0.034$ or 3.4 %

$P_f=0.0049$ or 0.49 %

The substrate contribution to the resistive losses as a fraction of the generated power is given by

$$P_{substrate}=\frac{J_{MP}t\rho}{V_{MP}} \tag{20}$$

where ρ is the substrate resistivity and t the wafer thickness.

For a substrate resistivity of 1 ohm centimeter, t of 0.028 cm, V_{MP} of 550 mV and J_{MP} of 32.2 mA/cm^2,

$$p_{substrate}=0.16\ \% \tag{21}$$

For a double sided structure, the open circuit voltage is weakly dependent on the substrate resistivity (section 2).

The fractional resistive power losses for the RFJC can be summarized by the following equations [14]

$$P_{cathode}=\frac{J_{MP}}{V_{MP}}\left[\frac{(s-w)^2R_{s,\,emitter}}{12}+\frac{(s-w)L^2\rho m}{3A_f}+\rho_c\left(\frac{w_c}{s-w_f}\right)\right] \tag{22}$$

$$P_{anode}=\frac{J_{MP}}{V_{MP}}\left[\frac{(s-w)^2R_{s,\,substrate}}{12}+\frac{(s-w)L^2\rho m}{3A_f}+\rho_c\left(\frac{w_c}{s-w_f}\right)\right] \tag{23}$$

where

s is the center-to-center distance between adjacent fingers,

w the width of metal finger,

W_c is the width of the metal/silicon contact in the grooves,

$R_{s,\,emitter}$ the sheet resistance of the emitter

$R_{s,\,substrate}$ is the sheet resistance of the substrate

L is the length of the fingers

A_f is the cross-sectional area of the fingers

ρ_m is the resistivity of the plated copper

ρ_c is the effective contact resistance of metal/silicon interface

t is the thickness of the substrate (or the Silicon Wafer)

$p_{cathode}$ is the fractional resistive power loss associated with the cathode

p_{anode} is the fractional resistive power loss associated with the anode

$p_{substrate}$ is the upper limit of the fractional resistive power loss associated with the perpendicular flow of current across the substrate

Therefore, the total resistive loss in RFJC is given by

$$p_{resistive}=p_{cathode}+p_{anode}$$

$p_{resistive}$ is the total fractional resistive power loss when the cell is at operating current J and voltage V.

By substituting appropriate values into equations 22 and 23, the total resistive losses can be estimated as 2.95 %. This estimate

assumes the front and rear fingers to be of the same spacing.

7. Rear contact design

The rear contact for the RFJC is the p^{++} grooves. The major consideration for the rear design was to reduce the dark saturation current to a value far less than that obtained for the SSBC. This can be achieved by having fewer grooves (fingers) on the rear. This would minimize rear contact recombination, maximizing the V_{OC} and J_{SC}. However, this would have less desirable effects upon the contact resistance and the resistance due to lateral flow of light generated carriers in the bulk, reducing the cell fill factor. Since shading losses are not as important for the rear of the cell, the aspect ratio is also less important. However, since the p^{++} region through boron diffusion is unknown, the initial rear finger contact spacing is set to being equal to the front grid.

8. Efficiency estimates including shading and resistive losses

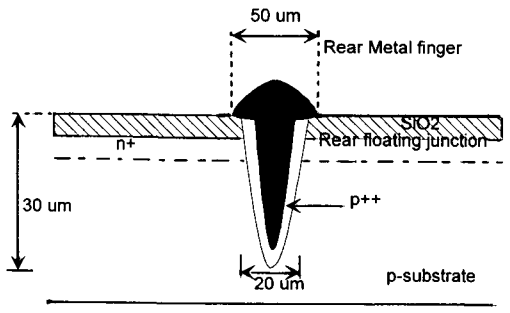

Fig. 5. Schematic of rear contact for RFJC.

The effect of shading and resistive losses on the previously estimated efficiency in section 4 are as follows. As calculated in section 6, the total shading loss of 2.95 % reduces the short circuit current to 38.8 mA/cm^2, and the open circuit voltage of 685 mV is obtained. The resistive loss of 2.95 % reduces the fill factor to 80.9 %. These parameters correspond to an efficiency of 21.5 % as being a realistically achievable efficiency for RFJC. This value is clearly a function of the diffusion length. If the diffusion length, which depends on starting wafer, cleanliness of processing, presence of gettering steps, avoidance of dislocations etc., is either increased (above 1.35 mm) or decreased, then the efficiency will accordingly either rise or fall.

It should be noted, that well passivated surfaces facilitate application to thinner substrates without performance loss. This can be particularly important for low quality commercial substrates, where the normally high dark saturation current contribution from the substrate can be minimized by reducing the thickness.

9. Discussion and conclusion

The RFJC structure provides an improved rear surface passivation without the use of photolithography. This provides a way of overcoming the performance limitation imposed on the SSBC cell by the aluminum alloyed rear region. The RFJC structure is capable of yielding very high open circuit

voltages in comparison to SSBC structure because of the lower effective back surface recombination velocity associated with the rear floating junction.

Estimates of contribution to the total dark saturation current density have been made and used for efficiency calculations using PC-1D. The efficiency value of 22.9 % was found realizable if limited only by groove recombination. However, 21.5 % efficiency was estimated as a more realistically achievable efficiency when the shading and the resistive power losses in the cell are taken into account.

It should be pointed out that, the estimated value can be exceeded if the photolithography technology is used to fabricate the RFJC and without the rear fingers but a PERF type of structure [16]. This is due to the elimination of the groove contributions to the dark saturation current density. However, as a commercial cell with simplicity and lower cost of production the 21.5 % efficiency is quite good.

Acknowledgment

We are thankful to other Photovoltaics Project members for their various contribution to this work.

References

[1] J. Zhao, A. Wang, S.R. Wenham and M.A. Green, 11th European Communities Photo Boltaic Solar Energy Conference, Montreux (1992).

[2] A.G. Aberle, S. Glunz and W. Warta J. Appl. Phys. 71(9) (1992) 4422.

[3] S.R. Wenham, M.A. Green and J. Zhao, 11th European Communities Photovoltaic Solar Energy Conference, Montreux (1992).

[4] A.U. Ebong, S.H. Lee, C.B. Honsberg and S.R. Wenham, Jpn. J. Appl. Phys. 35(4A) (1996) 2077

[5] S.R. Wenham, Y. Wu, R.D. Xiao, M. Taouk, M. Guelden, M.A. Green and D. Hogg, '11th European Communities Photovoltaic Solar Energy Conference, Montreux (992).

[6] A.U. Ebong, Ph.D. Thesis, The University of New South Wales, Sydney, Australia (1994).

[7] S.R. Wenham ,Ph.D. Thesis, The University of New South Wales, Sydney, Australia (1986).

[8] S.M. Sze, Semiconductor Devices, Physics and Techonlogy (John Wiley & Sons, New York, 1985).

[9] A.U. Ebong, S.H. Lee, W. Warta, C. Honsberg and S.R. Wenham, submitted to Solar Energy Materials and Solar Cells, June 1996.

[10] P. Basore, IEEE Trans. Electron Devices, ED-37 (1990) p. 337.

[11] C.B. Honsberg and S.R. Wenham, Progress in Photovoltaics, Vol. 3 (1995) 79-87.

[12] A.B. Sproul, M.A. Green and A.M. Robinson, Solar Cells 28 (1990) 233.

[13] J. Zhao, A. Wang and M.A. Green,

Progress in Photovoltaics (1995).

[14] M. Taouk, Ph.D. Thesis, The University of New South Wales (1993).

[15] M.A. Green, Solar Cells : Operating Principles, Technology and System Applications, (Prentice-Hall, Inc., Englewood Cliffs, N.J., 1982).

[16] S.R. Wenham, S.J. Robinson, X. Dai, J. Zhao, A. Wang, Y.H. Tang, A. Ebong, C.B. Honsberg and M.A. Green, Conf. Proc., 24th IEEE Photovoltaic Specialists Conference, Waikoloa-Hawaii, December (1994) 1278.

[17] Y.M. Ghannam, Conf. Record, 21st IEEE Specialist Conference, Las Vegas (1991) p. 284.